Axion Dark Matter Search around 4.55 μeV with Dine-Fischler-Srednicki-Zhitnitskii Sensitivity

Andrew K. Yi,[1,2] Saebyeok Ahn,[1,2] Çağlar Kutlu,[1,2] JinMyeong Kim,[1,2] Byeong Rok Ko,[2,*] Boris I. Ivanov,[2] HeeSu Byun,[2] Arjan F. van Loo,[3,4] SeongTae Park,[2] Junu Jeong,[2] Ohjoon Kwon,[2] Yasunobu Nakamura,[3,4] Sergey V. Uchaikin,[2] Jihoon Choi,[2,†] Soohyung Lee,[2] MyeongJae Lee,[2,‡] Yun Chang Shin,[2] Jinsu Kim,[1,2] Doyu Lee,[2,§] Danho Ahn,[1,2] SungJae Bae,[1,2] Jiwon Lee,[1,2] Younggeun Kim,[2] Violeta Gkika,[2] Ki Woong Lee,[2] Seonjeong Oh,[2] Taehyeon Seong,[2] DongMin Kim,[2] Woohyun Chung,[2] Andrei Matlashov,[2] SungWoo Youn,[2] and Yannis K. Semertzidis[2,1]

[1]*Department of Physics, Korea Advanced Institute of Science and Technology, Daejeon 34141, Republic of Korea*
[2]*Center for Axion and Precision Physics Research, Institute for Basic Science, Daejeon 34051, Republic of Korea*
[3]*RIKEN Center for Quantum Computing (RQC), Wako, Saitama 351-0198, Japan*
[4]*Department of Applied Physics, Graduate School of Engineering, The University of Tokyo, Bunkyo-ku, Tokyo 113-8656, Japan*

We report an axion dark matter search at Dine-Fischler-Srednicki-Zhitnitskii sensitivity with the CAPP-12TB haloscope, assuming axions contribute 100% of the local dark matter density. The search excluded the axion-photon coupling $g_{a\gamma\gamma}$ down to about 6.2×10^{-16} GeV^{-1} over the axion mass range between 4.51 and 4.59 μeV at a 90% confidence level. The achieved experimental sensitivity can also exclude Kim-Shifman-Vainshtein-Zakharov axion dark matter that makes up just 13% of the local dark matter density. The CAPP-12TB haloscope will continue the search over a wide range of axion masses.

The standard model of big bang cosmology combined with precision cosmological measurements strongly suggests that cold dark matter (CDM) constitutes about 85% of the matter and 27% of the energy density in the Universe [1]. CDM is a subject of beyond the standard model of particle physics (SM) and remains hidden to date. The axion [2] stems from the breakdown of a new global symmetry introduced by Peccei and Quinn [3] to solve the strong CP problem in the SM [4], and is one of the most prominent CDM candidates, provided its mass is above $\mathcal{O}(\mu\text{eV})$ according to the original work [5], or above $\mathcal{O}(\text{peV})$ by more recent works [6], and below $\mathcal{O}(\text{meV})$ [7,8].

The axion haloscope search proposed by Sikivie [9] exploits the axion-photon coupling $g_{a\gamma\gamma}$ in a microwave cavity permeated with a static magnetic field, which results in resonant conversions of axions to photons when the axion mass m_a matches the frequency of the cavity mode ν, $m_a = h\nu/c^2$. The two most popular models, Kim-Shifman-Vainshtein-Zakharov (KSVZ) [10] and Dine-Fischler-Srednicki-Zhitnitskii (DFSZ) [11], benchmark the $g_{a\gamma\gamma}$ with $g_\gamma = -0.97$ and 0.36, respectively, where g_γ is a dimensionless coupling constant and comes from $g_{a\gamma\gamma} = (\alpha g_\gamma/\pi f_a)$ along with the axion decay constant f_a and the fine structure

constant α. The use of a high-quality microwave cavity makes the axion haloscope the most promising method for axion dark matter searches in the microwave region.

In this Letter, we report a DFSZ axion dark matter search using the CAPP-12TB haloscope at the Institute for Basic Science Center for Axion and Precision Physics Research (CAPP) [12,13]. Here, 12TB stands for our solenoid specifications, the central magnetic field of 12 T and the Big bore of 320 mm [14]. To date, DFSZ axion dark matter sensitive searches were only achieved by the Axion Dark Matter eXperiment (ADMX) [15,16].

The CAPP-12TB haloscope depicted in Fig. 1 comprises a 36.85 L frequency tunable copper cylindrical cavity placed at the magnet center, a superconducting solenoid whose rms magnetic field B_{rms} over the cavity volume V is 10.31 T, and a heterodyne receiver chain with a Josephson
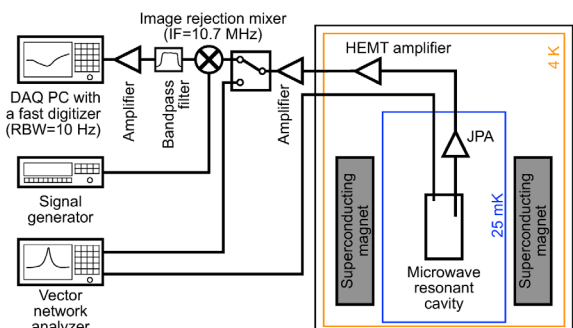

FIG. 1. Schematic of the CAPP-12TB haloscope.

parametric amplifier (JPA) as the first amplifier. The experiment maintained the physical temperatures of the cavity and the JPA at around 25 mK using a dilution refrigerator DRS-1000 [17] whose cooling power was measured to be about 1 mW at 90 mK without any load.

The detected axion signal power is expected to be

$$P_a^{a\gamma\gamma} = 22.51 \text{ yW} \left(\frac{g_\gamma}{0.36}\right)^2 \left(\frac{B_{\text{rms}}}{10.31 \text{ T}}\right)^2$$
$$\times \left(\frac{V}{36.85 \text{ L}}\right) \left(\frac{C}{0.6}\right) \left(\frac{Q_L}{35\,000}\right)$$
$$\times \left(\frac{\nu}{1.1 \text{ GHz}}\right) \left(\frac{\rho_a}{0.45 \text{ GeV/cm}^3}\right) \qquad (1)$$

when the axion mass matches the frequency of the cavity mode $m_a = h\nu/c^2$ and the cavity mode coupling to the receiver, β, is 2. In Eq. (1), C is the cavity-mode-dependent form factor which in practice includes the axion-photon interaction energy normalized by the energy stored in the electric and magnetic fields over the cavity volume [18], Q_L is the loaded quality factor of the cavity mode, and ρ_a is the local dark matter density. Here, we have assumed axions make up 100% of the local dark matter density, i.e., $\rho_a = 0.45$ GeV/cm^3, to explore the $g_{a\gamma\gamma}$. As the CAPP-12TB axion haloscope has cylindrical geometry, the chosen cavity mode for this search is the TM$_{010}$-like mode, to maximize C. Assuming the standard halo model of axion dark matter, the signal power given in Eq. (1) would then be distributed over a boosted Maxwellian shape with an axion rms speed of about 270 km/s, and the Earth rms speed of 230 km/s with respect to the galaxy frame [19], respectively, which is the model for this work.

We have realized a frequency tuning mechanism operating in a cryogenic and high-magnetic-field environment employing a piezoelectric motor manufactured by attocube [20]. The motor sits on the top end cap of the cavity and links the tuning rod directly through a crank arm, where the tuning rod is a copper cylinder whose diameter is about a tenth of the cavity diameter. By rotating the tuning rod about the tuning axle, we tuned the cavity modes over the frequency range considered in this work. Another attocube piezoelectric motor for an antenna has been adopted to adjust β that was measured to be 1.8–2.2 during data taking through the "Strong" line in Fig. 2. A fixed antenna minimally coupled to the cavity has also been implemented at the end of the "Weak" line. The Q_L of the TM$_{010}$-like mode for each frequency step was measured to be 35 000–38 000, and the relevant unloaded cavity quality factor $Q_0 = Q_L(1 + \beta)$ was 107 000–114 000, and the mode-dependent C were calculated to be about 0.6 using a finite element method calculation [21].

Our receiver chain consists of a single data acquisition (DAQ) channel. As shown in Fig. 2, power from the cavity goes through a directional coupler, two circulators, and a
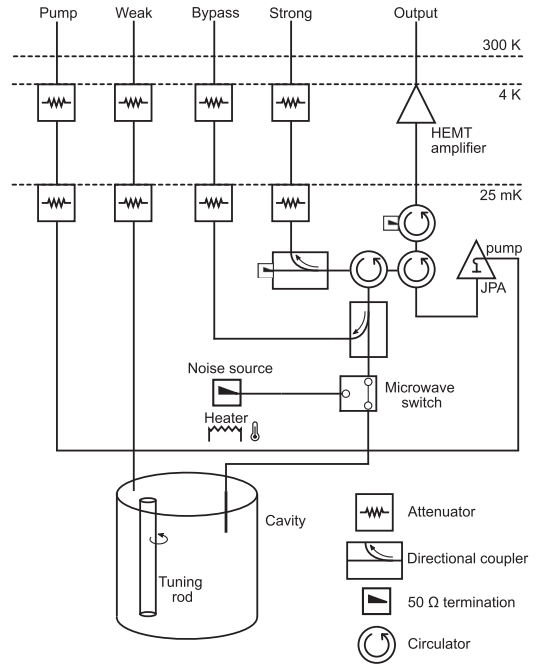

FIG. 2. CAPP-12TB receiver diagram.

JPA, which were located in the magnetic-field cancellation region realized by a magnet system [14].

The JPA is described and characterized in detail elsewhere [22,23], and here we describe our JPA operation scheme for this work. The JPA profiles were probed with a +1 kHz offset from the JPA resonant frequencies which were set according to the target frequencies with a −100 kHz offset, where the target frequencies are the central frequencies of each individual power spectra. The JPA gains G_{JPA}, detailed in Appendix A, were measured through the "Bypass" line including a 50-Ω termination (the "Noise source" in Fig. 2) by the microwave switch. They were about 17 dB at the target frequencies over the frequency range. The noise temperatures of the JPA T_{JPA} were measured to be about 60 mK at the target frequencies from the power ratio with and without JPA amplification [16] (see also Appendix A). The in situ G_{JPA} through the line including the cavity instead of the 50-Ω termination were measured every time the cavity was tuned during data collection. The power was further amplified inside the fridge using two serial LNF-LNC0.6_2A [24] high-electron-mobility transistor (HEMT) amplifiers anchored at the 4-K stage.

After further processing outside the fridge (see also Fig. 1), which is comprised of down conversion to the intermediate frequency (IF) of 10.7 MHz with an image rejection mixer [25] and additional amplification, the power was then digitized and converted into a frequency spectrum over a span from −500 to +500 kHz with respect to the IF with a resolution bandwidth (RBW) of 10 Hz utilizing the fast DAQ system [26], accessed via CULDAQ [27].

The gain and noise temperature from the receiver chain other than the JPA, $G_{\text{JPA}_{\text{off}}}$, and $T_{\text{JPA}_{\text{off}}}$ were measured using

the Y-factor method [28] by varying the physical temperature of the "Noise source" up to 400 mK without JPA amplification. Accordingly they include all the attenuation and noise from the rest of the chain and are about 104 dB and 1.2 K, respectively, where the latter contributes about 25 mK to the noise temperature measurements with the 50-Ω termination according to Ref. [29] at the target frequencies. The total gain of the receiver chain including the *in situ* G_{JPA} of about 17 dB, G_{total}, is about 121 dB at the target frequencies.

The total system noise temperature T_n, detailed in Appendix B, was obtained from every individual power spectra by eliminating the G_{total} in power and then parametrized with a Savitzky-Golay (SG) filter [30]. The parameters of the SG filter were a polynomial of degree 4 and a 2001-point window at an RBW of 10 Hz. The extracted T_n at the cavity mode ν is about 215 mK as an approximately Lorentzian peak (see Fig. 6 in Appendix B), which is attributed to the tuning rod being hotter than the cavity walls due to the poor thermal link between them and the piezoelectric motor operation for the frequency tuning.

The signal-to-noise ratio (SNR) in this work is defined by the signal power for the DFSZ axion dark matter coupling $g_{a\gamma\gamma}^{DFSZ}$

$$\text{SNR} = \frac{P_a^{g_{a\gamma\gamma}^{DFSZ}}}{P_n}\sqrt{b_a \Delta t} = \frac{P_a^{g_{a\gamma\gamma}^{DFSZ}}}{k_B b_a T_n}\sqrt{N} = \frac{P_a^{g_{a\gamma\gamma}^{DFSZ}}}{\sigma_{P_n}} \quad (2)$$

according to the radiometer equation [31], where P_n and σ_{P_n} are the total noise power and its fluctuation, respectively. b_a is the axion signal window, Δt is the integration time at each step, N is the number of power spectra, and k_B is the Boltzmann constant. We acquired data from March 1 to March 18 in 2022 including system maintenance. A total of 1996 resonant frequencies were scanned over a search range of 20.06 MHz with frequency steps of 10 kHz, except for 380 kHz due to the mode crossings around an axion mass of 4.527 μeV. We made sure that the cavity simulation [21] also observed the mode crossings. Power spectra were taken with $\Delta t \sim 500$ s at each step, which resulted in $N \sim 5000$ with our RBW choice of 10 Hz [26]. The power spectra were averaged and then processed through the analysis procedure addressed below. The expected SNR values over the search range were generally higher than 5.

The data analysis process basically follows the axion haloscope analysis procedures developed to date [32–34]. From each power spectrum, only the axion signal sensitive region around the cavity mode was used. Furthermore, a span of 150 kHz centered at the target frequency was selected to avoid the presence of the pump tone and higher noise contribution with lower JPA gain [29]. The frequency span allows 15 power spectra to overlap in most of the frequency range with our frequency steps of 10 kHz. First, narrow spikes in each power spectrum were removed with a filtering procedure similar to the one by the Haloscope At Yale Sensitive To Axion CDM [33]. Each power spectrum

was parametrized by a χ^2 fit and then went through the filtering at an RBW of 10 Hz. The fit function is the product of a five-parameter function [32] for the overall noise profile of the cavity and the receiver chain, a Lorentzian for the G_{JPA} profile, and a quadratic or, equivalently, inverse Lorentzian for the noise profile depending on the G_{JPA} profile (Fig. 6 in Appendix B shows a hint of this dependence). In the fit, the minimum of the quadratic function was constrained to be located at the JPA resonant frequency according to the G_{JPA} profile, and the JPA gain at the target frequency was required to be consistent with the aforementioned measurement. This χ^2 parametrization improved the SNR efficiency ϵ_{SNR} by about 10% in the end albeit having almost the same rescan candidates compared to that by an SG filter using the same parameters mentioned above. Five nonoverlapping frequency points in each power spectrum were merged for further filtering at RBW of 50 Hz and the background subtraction thereafter. After the background subtraction, each power spectral line and its fluctuation in each spectrum were scaled by the expected total axion signal power, where the scaling across the spectrum follows the Lorentzian line shape characterized by the cavity Q_L [33]. Allowing the overlaps among the power spectra, all the power spectra were then combined to produce a single power spectrum, and the associated power fluctuations were also propagated accordingly. The RBW of the combined spectrum was further reduced to 450 Hz by merging nine nonoverlapping frequency points, which reduced the SNR as discussed below. This was, however, a tradeoff to reduce the number of rescan candidates. From the combined spectrum, our "grand power spectrum" was constructed by coadding [32] nine adjacent 450 Hz power spectral lines. This corresponds to a b_a of 4050 Hz retaining more than 99.9% of the putative signal power of axion dark matter considered in this Letter. Each power spectral line in the grand power spectrum was weighted by the axion signal shape, a boosted Maxwellian [33]. The grand power spectrum was normalized by σ_{P_n} which was also weighted according to the signal shape [33] and coadded [32]. A frequency-independent scale factor of 0.94 was applied to remedy the bias in power excess induced from the background subtraction [34], resulting in a normalized grand power spectrum following the standard Gaussian as shown in Fig. 3(a). With such standard Gaussian statistics, we applied a threshold of $3.718\sigma_{P_n}$ which is not only to get a one-sided 90% upper limit corresponding to the expected axion signal power of $5\sigma_{P_n}$ from the CAPP-12TB experiment, but also manageable rescan candidates. We found 33 power spectral lines located in 14 individual power spectra exceeded the cut. After rescanning the 14 individual power spectra with sufficiently high statistics, no power spectral lines were found to exceed the cut.

The ϵ_{SNR} was estimated from 10 000 simulated CAPP-12TB experiments with axion signals at a particular
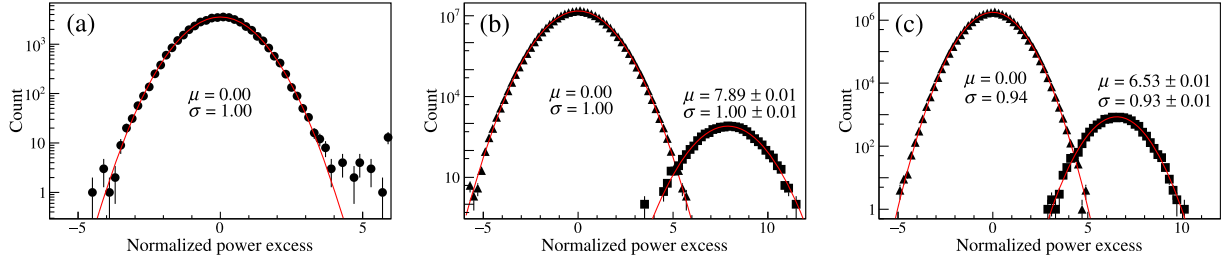
FIG. 3. Circles in (a) show the distribution of the normalized power excess from all the frequencies in the normalized grand power spectrum from the CAPP-12TB experiment, after applying a frequency-independent scale factor of 0.94 which is the original width of the distribution. (b) Distributions of the normalized power excess from 10 000 simulated CAPP-12TB experiments by coadding 81 adjacent 50 Hz power spectral lines after the background subtraction using the simulation input, and (c) those by nine adjacent 450 Hz power spectral lines and the χ^2 fit. Rectangles and triangles in (b) and (c) are from the frequency with the simulated axion signals and frequencies with background only, respectively, where both are from the same simulated signals with an initial signal-to-noise ratio of 7.89. Lines are a Gaussian fit resulting in μ (mean) and σ (width).

frequency on top of the CAPP-12TB background [34]. Figures 3(b) and 3(c) show the normalized power excess distributions from the simulation, where Fig. 3(b) was obtained by coadding 81 adjacent 50 Hz power spectral lines after the background subtraction using the simulation input, and Fig. 3(c) by nine adjacent 450 Hz power spectral lines and our χ^2 fit. The narrow width of the normalized power excess distribution 0.94 induced from the background subtraction shown in the CAPP-12TB data was also demonstrated by the large statistics simulation data, as shown in the solid triangles in Fig. 3(c). The ϵ_{SNR} at an RBW of 450 Hz with respect to the SNR at an RBW of 50 Hz is estimated to be 88% from the means of the rectangle distributions in Figs. 3(b) and 3(c), and also with the frequency-independent scale factor of 0.94. This

88% is attributed to not only the signal weighting in the coadding procedure with the reduced RBW from 50 to 450 Hz (95%) [35], but also the background subtraction (93%). The former implies that there is SNR degradation depending on the RBW choice, and the latter is our ϵ_{SNR} with respect to the SNR at an RBW of 450 Hz. Other SNR inefficiencies, from the filtering and the axion signal misalignment with respect to the RBW of 450 Hz, were negligible compared with that from the background subtraction [13]. The total ϵ_{SNR} taking into account for the background subtraction, the additional line attenuation (see Appendix C), and the systematic uncertainty (see Appendix B) were reflected in our exclusion limits.

We set the 90% upper limits of $g_{a\gamma\gamma}$ for $4.51 < m_a < 4.59$ μeV. Figure 4 shows the excluded parameter space at
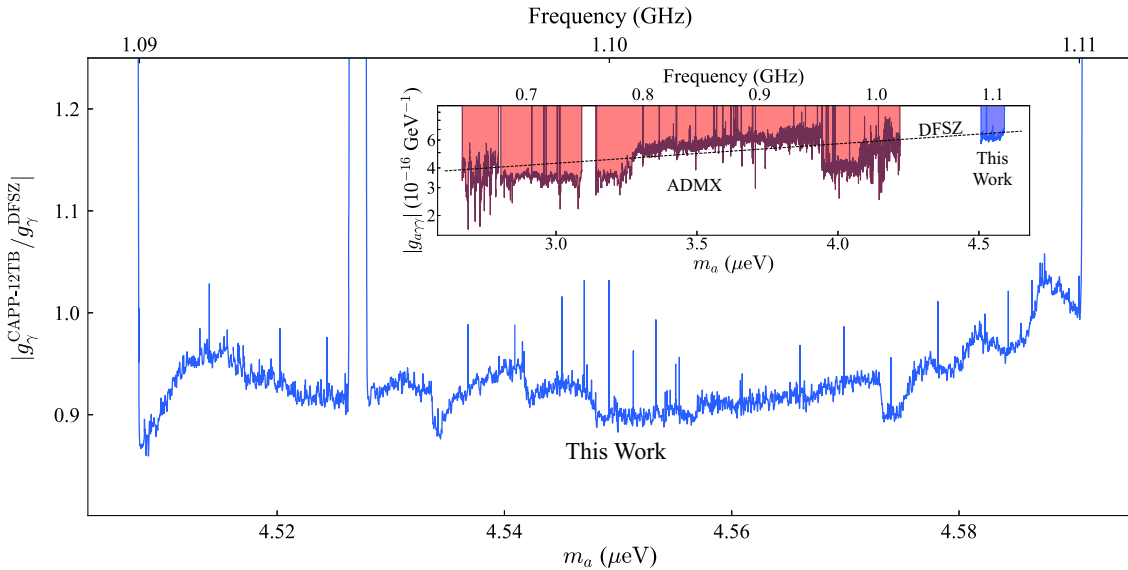

FIG. 4. Blue solid line is the excluded parameter space at a 90% confidence level by this work. Note the mode crossing around an axion mass of 4.527 μeV, which is predicted by a finite element method calculation [21]. The inset shows exclusion limits from other axion haloscope searches sensitive to the DFSZ axion dark matter [15,16] as well as that from this work. The intermittent spikes are less sensitive due to the filtering procedure (see the text) reducing statistics at the given frequency points.
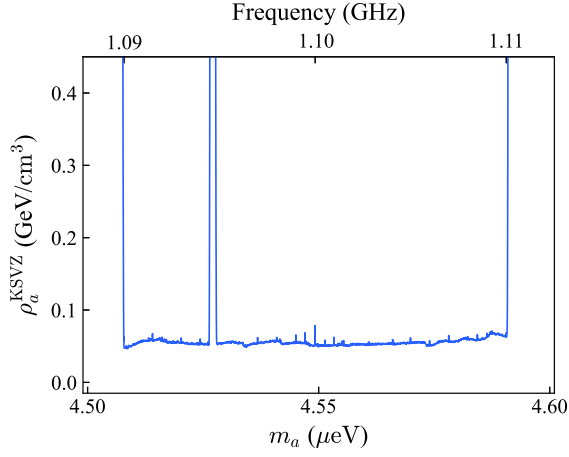
FIG. 5. Exclusion limits for the KSVZ axion dark matter density ρ_a^{KSVZ} at a 90% confidence level.

a 90% confidence level (CL) from the CAPP-12TB experiment. Using the achieved experimental sensitivity, we also excluded KSVZ axion dark matter, which makes up 13% of the ρ_a^{KSVZ}, as shown in Fig. 5. Our results are the most sensitive in the relevant axion mass range to date.

In summary, we report a search for DFSZ axion dark matter using the CAPP-12TB haloscope. The CAPP-12TB experiment has been pushing all the experimental parameters to reach state-of-the-art performance. With such performance, the CAPP-12TB experiment has achieved $g_{a\gamma\gamma}$ of about 6.2×10^{-16} GeV^{-1} which is beyond the DFSZ axion dark matter coupling, over the axion mass range between 4.51 and 4.59 μeV at a 90% CL. This is an unprecedented sensitivity tier in the mass range to date. We expect that CAPP-12TB as a state-of-the-art axion haloscope will continue sensitive searches over a wide range of axion masses with high-frequency [36] and high-quality cavity designs [37].

Appendix A: JPA gain and noise.—The JPA gains were measured with a vector network analyzer (VNA) as the power ratio with and without the pump power through the "Pump" line in Fig. 2 for the parametric amplification. Equation (A1) shows the relation between the power ratio and the JPA characteristics, T_{JPA} and G_{JPA}.

$$\frac{P_{\mathrm{JPA_{on}}}^{\mathrm{NS}}}{P_{\mathrm{JPA_{off}}}^{\mathrm{NS}}} = \frac{(T_{\mathrm{NS}} + T_{\mathrm{JPA}} + \frac{T_{\mathrm{JPA_{off}}}}{G_{\mathrm{JPA}}})G_{\mathrm{JPA}}}{T_{\mathrm{NS}} + T_{\mathrm{JPA_{off}}}}, \tag{A1}$$

where $P_{\mathrm{JPA_{on}}}^{\mathrm{NS}}$ and $P_{\mathrm{JPA_{off}}}^{\mathrm{NS}}$ are the powers transferred from a noise source (NS) with and without JPA

amplification, respectively, and T_{NS} and $T_{\mathrm{JPA_{off}}}$ are the noise temperatures from a NS and the receiver chain without JPA amplification, respectively. For the JPA gain measurement, the noise source was the VNA, and the power from the VNA was set much higher than other two power sources, satisfying the relation $(P_{\mathrm{JPA_{on}}}^{\mathrm{VNA}}/P_{\mathrm{JPA_{off}}}^{\mathrm{VNA}}) \simeq (T_{\mathrm{VNA}}G_{\mathrm{JPA}}/T_{\mathrm{VNA}}) = G_{\mathrm{JPA}}$. We required the JPA gains at the probe tones to be 20 ± 0.4 dB and thus always obtained gains of around 20 dB at the JPA resonant frequencies. Our target frequencies had a $+100$ kHz offset from the JPA resonant frequencies, so the *in situ* G_{JPA} for this axion dark matter search was about 17 dB at the cavity modes over the frequency range, while those at -100 and $+100$ kHz detuned from the cavity modes were about 20 and 14 dB, respectively, with JPA bandwidths of about 190 kHz.

The JPA noise temperatures were also measured using the power ratio with and without the JPA amplification, which also follows Eq. (A1). For the JPA noise temperature measurement, the noise source was the 50-Ω termination (denoted as "Noise source" in Fig. 2). The physical temperature of the 50-Ω termination was maintained at about 25 mK, resulting in a $T_{50-\Omega}$ of about 34 mK for the frequency range considered in this Letter according to the standard quantum limit. Hence, it is possible to extract the T_{JPA} from Eq. (A1) using two independent measurements, the aforementioned G_{JPA} and the $T_{\mathrm{JPA_{off}}}$ using the Y-factor method in the text, and the resulting $(T_{\mathrm{JPA_{off}}}/G_{\mathrm{JPA}})$ is about 25 mK at the target frequencies.

One can also extract the T_{JPA} by varying the physical temperature of the "Noise source," i.e., using the Y-factor method. We found that varying the physical temperature of the "Noise source" also varied G_{JPA}. This was why we were not able to apply the Y-factor method to get the reliable T_{JPA}. However, varying the physical temperature of the 50-Ω termination from 100 to 400 mK did not affect the HEMT physical temperature. It enabled us to apply the Y-factor method for the $T_{\mathrm{JPA_{off}}}$ measurements.

Appendix B: Total noise.—Equation (B1) shows the relation between the measured power transferred from the cavity, the total system noise temperature T_n, and the total system gain G_{total}.

$$P_{\mathrm{JPA_{on}}}^{\mathrm{cavity}} = k_B \Delta f T_n G_{\mathrm{total}}, \tag{B1}$$

where Δf is the RBW. Figure 6 shows a typical T_n as a function of frequency down-converted to the IF at a particular frequency step, after eliminating the G_{total} from the measured power $P_{\mathrm{JPA_{on}}}^{\mathrm{cavity}}$. As shown in Fig. 6, the total noise temperatures at -100 and $+100$ kHz detuned from the target frequency were typically 130 and 190 mK, which mainly comes from the Lorentzian JPA gain profile that determines the noise temperature profiles of the chain after the JPA [29] and of the JPA itself [see Eq. (A1)] as
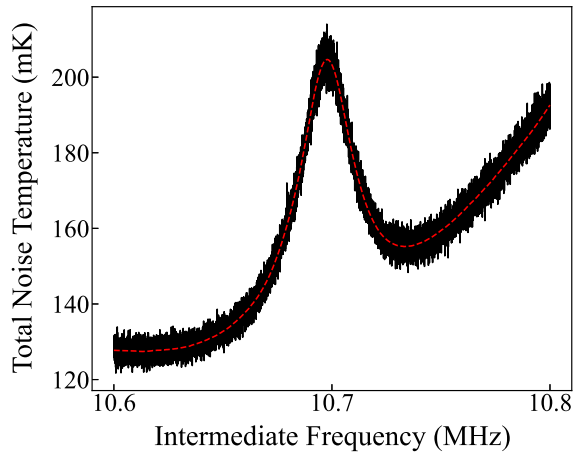
FIG. 6. $T_n = (P_{\mathrm{JPA_{on}}}^{\mathrm{cavity}}/k_B \Delta f G_{\mathrm{total}})$ as a function of frequency from a particular frequency step. Red dashed lines represents the SG filter parametrization of T_n.

well. Considering the noise profile comes from the Lorentzian JPA gain profile, the T_n around the target frequency is about 140 mK. A naïve estimate of the T_n from the aforementioned measurements with the "Noise source" is about 120 mK which is a sum of the noise contributions shown in the parentheses in Eq. (A1), where they are 34, 60, and 25 mK, respectively. In this case, the noise source is the cavity. We admit that there is a 20 mK difference from the physical temperature difference between the cavity top and bottom due to the incomplete thermalization between the cavity walls and the hot tuning rod, where the two temperatures are 25 and 45 mK, respectively. Provided the cavity noise temperature on average is about 10 mK higher than that from the cavity top, the 20 mK difference can roughly be understood, since this additional noise temperature contributes also to the JPA input referred noise at the idler frequency [38]. Nevertheless, our total noise temperature measurement is inclusive and does not distinguish the three contributions shown in the parentheses in Eq. (A1). Therefore, our resulting sensitivity is reliable, in spite of the lack of the exact cavity temperature information, with an accurate G_{total} corrected in Appendix C. In our inclusive T_n measurement, the uncertainty of our temperature sensor RX-C102B [39] for the 50-Ω termination as the "Noise source" in Fig. 2 can contribute to the "Noise source" temperatures in $G_{\mathrm{JPA_{off}}} = P_h - P_c/k_B \Delta f (T_h - T_c)$, where P_h and P_c are the powers transferred from the "Noise source" whose temperatures are T_h (400 mK) and T_c (100 mK), respectively, without the JPA amplification, thus affecting G_{total}. The magnetic-field-dependent temperature sensor error is expected to be negligible [39], because it was located in the magnetic-field cancellation region realized by the magnet system [14]. The relevant data are limited down to a temperature of $\mathcal{O}(1 \text{ K})$, but the errors at below a magnetic field of 1 T are less than

1% and independent of the physical temperature of the sensor [39]. Nonetheless, we conservatively assigned the sensor error of 2% which propagated to about 3% to $G_{\mathrm{JPA_{off}}}$, subsequently to T_n.

With the cavity as a noise source, the T_n was also measured using Eq. (A1), $(P_{\mathrm{JPA_{on}}}^{\mathrm{cavity}}/P_{\mathrm{JPA_{off}}}^{\mathrm{cavity}}) = T_n G_{\mathrm{JPA}}/T_{\mathrm{cavity}} + T_{\mathrm{JPA_{off}}}$. Here, the T_n was extracted inclusively with two other measurements, the aforementioned G_{JPA} and the $T_{\mathrm{JPA_{off}}}$ from the Y-factor method in the text. We found the difference between the two T_n values was at most 5% due to imperfections in our measurements. Otherwise, they are likely consistent with each other because the two measurements are almost fully dependent.

The total systematic uncertainty of our T_n measurement was estimated to be 6% by combining the two sources above.

Appendix C: Additional line attenuation.—The line attenuation from the cavity to the microwave switch was not considered in our total gain G_{total} mentioned in the text. Using a VNA and "Strong" line in Fig. 2, we measured two reflected powers, one from the cavity and the other from the switch. In order to obtain the fully reflected power, the switch was configured to float between the two switch ports, and the cavity off resonant frequency range was inspected. The line attenuation was measured by taking half of the difference between the two reflection measurements and was 0.3–0.5 dB depending on the frequency.

*Corresponding author.
brko@ibs.re.kr
†Present address: Korea Astronomy and Space Science Institute, Daejeon 34055, Republic of Korea.
‡Present address: Department of Physics, Sungkyunkwan University, Suwon 16419, Republic of Korea.
§Present address: Samsung Electronics, Gyeonggi-do 16677, Republic of Korea.

[1] P. A. R. Ade *et al.* (Planck Collaboration), Astron. Astrophys. **594**, A13 (2016).
[2] S. Weinberg, Phys. Rev. Lett. **40**, 223 (1978); F. Wilczek, Phys. Rev. Lett. **40**, 279 (1978).
[3] R. D. Peccei and H. R. Quinn, Phys. Rev. Lett. **38**, 1440 (1977).
[4] G. 't Hooft, Phys. Rev. Lett. **37**, 8 (1976); Phys. Rev. D **14**, 3432 (1976); **18**, 2199(E) (1978); J. H. Smith, E. M. Purcell, and N. F. Ramsey, Phys. Rev. **108**, 120 (1957); W. B. Dress, P. D. Miller, J. M. Pendlebury, P. Perrin, and N. F. Ramsey, Phys. Rev. D **15**, 9 (1977); I. S. Altarev *et al.*, Nucl. Phys. **A341**, 269 (1980).
[5] J. Preskill, M. B. Wise, and F. Wilczek, Phys. Lett. **120B**, 127 (1983); L. F. Abbott and P. Sikivie, Phys. Lett. **120B**, 133 (1983); M. Dine and W. Fischler, Phys. Lett. **120B**, 137 (1983).

[6] F. Takahashi, W. Yin, and A. H. Guth, Phys. Rev. D **98,** 015042 (2018); P. W. Graham and A. Scherlis, Phys. Rev. D **98,** 035017 (2018).

[7] A. S. Sakharov and M. Yu. Khlopov, Yad. Fiz. **57,** 514 (1994) [Phys. At. Nucl. **57,** 485 (1994)]; A. S. Sakharov, D. D. Sokoloff, and M. Y. Khlopov, Yad. Fiz. **59N6,** 1050 (1996) [Phys. At. Nucl. **59,** 1005 (1996)]; M. Y. Khlopov, A. S. Sakharov, and D. D. Sokoloff, Nucl. Phys. B, Proc. Suppl. **72,** 105 (1999).

[8] J. Ellis and K. A. Olive, Phys. Lett. B **193,** 525 (1987); G. Raffelt and D. Seckel, Phys. Rev. Lett. **60,** 1793 (1988); M. S. Turner, Phys. Rev. Lett. **60,** 1797 (1988); H.-T. Janka, W. Keil, G. Raffelt, and D. Seckel, Phys. Rev. Lett. **76,** 2621 (1996); W. Keil, H. T. Janka, D. N. Schramm, G. Sigl, M. S. Turner, and J. Ellis, Phys. Rev. D **56,** 2419 (1997).

[9] P. Sikivie, Phys. Rev. Lett. **51,** 1415 (1983); Phys. Rev. D **32,** 2988 (1985).

[10] J. E. Kim, Phys. Rev. Lett. **43,** 103 (1979); M. A. Shifman, A. I. Vainshtein, and V. I. Zakharov, Nucl. Phys. **B166,** 493 (1980).

[11] A. R. Zhitnitskii, Yad. Fiz. **31,** 497 (1980) [Sov. J. Nucl. Phys. **31,** 260 (1980)]; M. Dine, W. Fischler, and M. Srednicki, Phys. Lett. **104B,** 199 (1981).

[12] Y. K. Semertzidis *et al.,* arXiv:1910.11591; J. Jeong, S. W. Youn, S. Bae, J. Kim, T. Seong, J. E. Kim, and Y. K. Semertzidis, Phys. Rev. Lett. **125,** 221302 (2020); O. Kwon, D. Lee, W. Chung, D. Ahn, H. S. Byun *et al.,* Phys. Rev. Lett. **126,** 191802 (2021); Y. Lee, B. Yang, H. Yoon, M. Ahn, H. Park, B. Min, D. L. Kim, and J. Yoo, Phys. Rev. Lett. **128,** 241805 (2022).

[13] S. Lee, S. Ahn, J. Choi, B. R. Ko, and Y. K. Semertzidis, Phys. Rev. Lett. **124,** 101802 (2020).

[14] W. Ma *et al.,* IOP Conf. Ser. **502,** 012104 (2019).

[15] N. Du, N. Force, R. Khatiwada, E. Lentz, R. Ottens *et al.* (ADMX Collaboration), Phys. Rev. Lett. **120,** 151301 (2018); T. Braine, R. Cervantes, N. Crisosto, N. Du, S. Kimes *et al.* (ADMX Collaboration), Phys. Rev. Lett. **124,** 101303 (2020).

[16] C. Bartram *et al.* (ADMX Collaboration), Phys. Rev. Lett. **127,** 261803 (2021).

[17] www.leidencryogenics.nl.

[18] B. R. Ko, H. Themann, W. Jang, J. Choi, D. Kim, M. J. Lee, J. Lee, E. Won, and Y. K. Semertzidis, Phys. Rev. D **94,** 111702(R) (2016).

[19] M. S. Turner, Phys. Rev. D **42,** 3572 (1990).

[20] www.attocube.com.

[21] www.cst.com; www.comsol.com.

[22] T. Yamamoto, K. Inomata, M. Watanabe, K. Matsuba, T. Miyazaki, W. D. Oliver, Y. Nakamura, and J. S. Tsai, Appl. Phys. Lett. **93,** 042510 (2008).

[23] Ç. Kutlu, A. F. van Loo, S. V. Uchaikin, A. N. Matlashov, D. Lee, S. Oh, J. Kim, W. Chung, Y. Nakamura, and Y. K. Semertzidis, Supercond. Sci. Technol. **34,** 085013 (2021).

[24] www.lownoisefactory.com.

[25] https://polyphasemicrowave.com.

[26] S. Ahn, M. J. Lee, A. K. Yi, B. Yeo, B. R. Ko, and Y. K. Semertzidis, J. Instrum. **17,** P05025 (2022).

[27] S. Lee, J. Phys. **898,** 032035 (2017).

[28] T. L. Wilson, arXiv:1111.1183.

[29] H. Friis, Proc. IRE **32,** 419 (1944).

[30] A. Savitzky and M. J. E. Golay, Anal. Chem. **36,** 1627 (1964).

[31] R. H. Dicke, Rev. Sci. Instrum. **17,** 268 (1946).

[32] S. J. Asztalos, E. Daw, H. Peng, L. J. Rosenberg, C. Hagmann *et al.,* Phys. Rev. D **64,** 092003 (2001).

[33] B. M. Brubaker, L. Zhong, S. K. Lamoreaux, K. W. Lehnert, and K. A. van Bibber, Phys. Rev. D **96,** 123008 (2017).

[34] S. Ahn, S. Lee, J. Choi, B. R. Ko, and Y. K. Semertzidis, J. High Energy Phys. 04 (2021) 297.

[35] Note also that the RBW reduction from 10 to 50 Hz decreases the SNR less than 0.1%.

[36] J. Jeong, S. Yoon, S. Ahn, J. E. Kim, and Y. K. Semertzidis, Phys. Lett. B **777,** 412 (2018).

[37] D. Ahn, O. Kwon, W. Chung, W. Jang, D. Lee, J. Lee, S. W. Youn, H. Byun, D. Youm, and Y. K. Semertzidis, Phys. Rev. Appl. **17,** L061005 (2022).

[38] J. Aumentado, IEEE Microw. Mag. **21,** 45 (2020).

[39] https://www.lakeshore.com.